

Structural changes in the hot Algol OGLE-LMC-DPV-097 and its disk related to its long-cycle

J. Garcés L.^{1*}, R.E. Mennickent¹, Djurašević^{2,3}, R. Poleski^{4,5}, I. Soszyński⁴

¹Universidad de Concepción, Departamento de Astronomía, Casilla 160-C, Concepción, Chile

²Astronomical Observatory, Volgina 7, 11060 Belgrade 38, Serbia

³Isaac Newton Institute of Chile, Yugoslavia Branch

⁴Warsaw University Observatory, Al. Ujazdowskie 4, 00-478 Warszawa, Poland

⁵Department of Astronomy, Ohio State University, 140 W. 18th Ave., Columbus, OH 43210, USA

ABSTRACT

Double Periodic Variables (DPVs) are hot Algols showing a long photometric cycle of uncertain origin. We report the discovery of changes in the orbital light curve of OGLE-LMC-DPV-097 which depend on the phase of its long photometric cycle. During the ascending branch of the long-cycle the brightness at the first quadrature is larger than during the second quadrature, during the maximum of the long-cycle the brightness is basically the same at both quadratures, during the descending branch the brightness at the second quadrature is larger than during the first quadrature and during the minimum of the long-cycle the secondary minimum disappears. We model the light curve at different phases of the long-cycle and find that the data are consistent with changes in the properties of the accretion disk and two disk spots. The disk's size and temperature change with the long-cycle period. We find a smaller and hotter disk at minimum and larger and cooler disk at maximum. The spot temperatures, locations and angular sizes also show variability during the long-cycle.

Key words: stars: binaries: close: eclipsing

1 INTRODUCTION

In the close interacting binaries Double Periodic Variables (DPVs) a giant fills its Roche lobe and transfers mass on to a B-type dwarf feeding an optically thick accretion disk. About 250 DPVs have been found in the Galaxy and the Magellanic Clouds (Poleski et al. 2010; Pawlak et al. 2013; Mennickent 2017). Typical orbital periods are few days and long-cycles last hundreds of days. The long-cycle lasts in average about 33 times the orbital period, but single period ratios run typically between 27 and 39. DPVs have been recently reviewed by Mennickent, Otero, & Kołaczkowski (2016) and Mennickent (2017).

The more enigmatic fingerprint of a DPVs is its long-cycle. It has been attributed to recurrent mass loss (Mennickent et al. 2008, 2012b). The triggering mechanism might be the magnetic dynamo of the rapidly rotating donor, that should modulate the mass transfer through the inner Lagrangian point (Schleicher & Mennickent 2017). A careful inspection of these hypotheses is needed in a number of systems before to validate them.

In this paper we present our analysis of the light curve of OGLE-LMC-DPV-097 ($\alpha_{2000} = 05:34:18.06$, $\delta_{2000} = -70:38:08.7$; MACHO 11.8746.65, 2MASS J05341808-7038087). This object is classified as a Double Periodic Variable with orbital period

$7^d.751749 \pm 0^d.000202$ and long-cycle $302^d.622 \pm 0^d.109$ by Poleski et al. (2010). OGLE-LMC-DPV-097 has one of the largest amplitude long-cycles among DPVs, viz. 0.717 mag in the I band. In this paper we extend the data analyzed by Poleski et al. (2010) including OGLE-IV photometry and present new and interesting results potentially useful to explain the DPV phenomenon.

2 PHOTOMETRIC DATA

The photometric time-series analyzed in this paper are taken from the OGLE-III/IV project databases¹. The OGLE-IV project is described by Udalski, Szymański, & Szymański (2015). The whole dataset, summarized in Table 1, spans a time interval of 4569 days, i.e. 12.5 years.

3 RESULTS

3.1 Light curve disentangling

We disentangled the light curve into an orbital and long-cycle part with the aid of a Fourier decomposition algorithm described by

* E-mail: jgarcetesletier@gmail.com

¹ OGLE-III/IV data kindly provided by the OGLE team.

Table 1. Summary of survey photometric observations. The number of measurements, starting and ending times for the series and average magnitude are given. HJD zero point is 2450000. Single point uncertainties are between 4 and 6 mmag.

Database	N	HJD _{start}	HJD _{end}	mag	band
III	443	2167.89750	4954.53850	16.086	<i>I</i>
IV	580	5260.63876	6736.62011	16.140	<i>I</i>

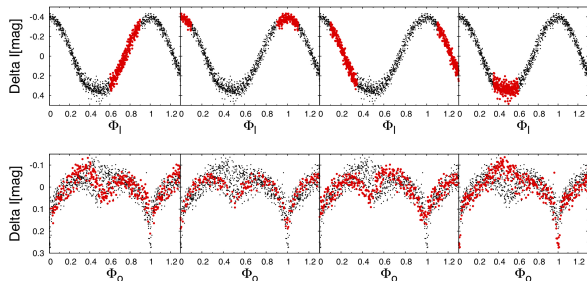


Figure 1. Disentangled long-cycle (up) and orbital (down) light curves phased with the respective periods. Black dots show the complete dataset, red dots show segments of the data of the long-cycle. It is evident the change in orbital light curve shape at different long-cycle phases.

Mennickent et al. (2012a) and the ephemerides for the orbital and long periods given by Poleski et al. (2010). The orbital and long-cycle light curves phased with the respective periods show an interesting behaviour that can be summarized as (Fig. 1): (a) during the ascending branch of the long-cycle the brightness at the first quadrature ($\Phi_o = 0.25$) is larger than during the second quadrature ($\Phi_o = 0.75$), (b) during the maximum of the long-cycle the brightness is basically the same at both quadratures, (c) during the descending branch the brightness at the second quadrature ($\Phi_o = 0.75$) is larger than during the first quadrature ($\Phi_o = 0.25$) and (d) during the minimum of the long-cycle the secondary minimum disappears. Furthermore, we have found that the variability is larger around the eclipses and it occurs smoothly during the long-cycle (Fig. 2)

The above behaviour suggests that there are structural changes in the binary (stars, gas stream, disk, circumstellar matter) related to the long-cycle. This is a strong constraint for any competent model intending to explain the long-cycle in this DPV.

3.2 Light curve model

In order to qualitatively understand the orbital light changes we separately analyzed the orbital light curves on the ascending, top, descending and minimum branches with a program developed by Djurašević (1992) which implements a sophisticated and versatile binary star model based on Roche geometry. This program has been used and tested for more than two decades on a wide range of binary configurations (e.g. Djurašević et al. 2010; Mennickent et al. 2015). The system parameters that best fit the observed light curve are estimated using the Marquart-Levenberg algorithm (Marquardt 1963) with modifications described in Djurašević (1992) to minimize the sum of squared residuals between the observed (O) and calculated (C) light curves.

In absence of spectroscopic data we use educated approximations to model the system. OGLE-LMC-DPV-097 has MACHO

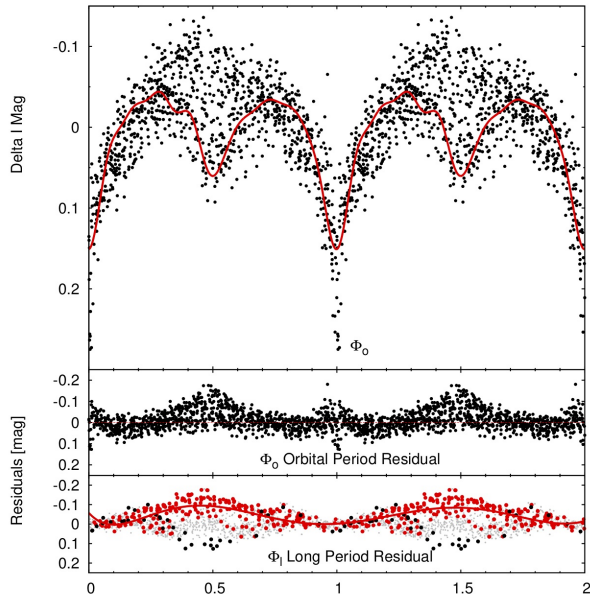


Figure 2. The upper panel shows the orbital light curve and a fit to the data obtained on maximum (red line). The middle panel shows the residuals of the fit, indicating that the larger variability occurs on times of eclipses. The bottom panel shows the same residuals that above, but in the x-axis the long-cycle phase is shown. Red points are data taken around the secondary eclipse ($0.45 \leq \Phi_o \leq 0.55$) and black points around the main eclipse ($0.98 \leq \Phi_o \leq 1.02$); the changes in the eclipses depth occur smoothly during the long-cycle.

catalogue² colour $V - R = -0.046$ so we use $T_1 = 14$ kK for the gainer. In addition, we assume synchronous rotation for the stellar components and $q = 0.2$. Based on the studied systems these figures can be considered representative for a DPV (Mennickent, Otero, & Kołaczowski 2016). With this approximation, we don't intend to get accurate system parameters for our system, at least not in this study, but to get a qualitative description of the *differential changes* occurring in the system during the long-cycle. For this reason we don't focus on the absolute stellar properties in this paper. A trial using $q = 0.15$ gives similar qualitative results to reported in this paper and suggests typical errors of 20 per cent for the disk radius, temperature and spots temperature ratio.

Following earlier work with DPVs, our model assumes an optically and geometrically thick disk. The disk edge is approximated by a cylindrical surface. The thickness of the disk can change linearly with radial distance, allowing the disk to take a conical shape (convex, concave or plane-parallel). The geometrical properties of the disk are determined by its radius (R_d), its thickness at the edge (d_e) and the thickness at the centre (d_c). The cylindrical edge of the disk is characterized by its temperature, T_d , and the conical surface of the disk by a radial temperature profile that follows the temperature distribution proposed by Zola (1991):

$$T(r) = T_d + (T_h - T_d) \left[1 - \left(\frac{r - R_h}{R_d - R_h} \right) \right]^{\sigma \tau} \quad (1)$$

We assume that the disk is in physical and thermal contact with the gainer, so the inner radius and temperature of the disk are

² <http://vizier.u-strasbg.fr/viz-bin/VizieR>

equal to the temperature and radius of the star. The temperature of the disk at the edge (T_d) and the temperature exponent (a_T), as well as the radii of the star (R_h) and of the disk (R_d) are free parameters, determined by solving the inverse problem. We refined the model of the system by introducing hot active regions on the edge of the disk. Our model includes two such active regions: a hot spot (hs) and a bright spot (bs). These regions are characterized by their temperatures, angular dimensions and longitudes. These parameters are also determined by solving the inverse problem and are given in Table 2. The models are compared with the observations in Figs. 3 and 4.

4 DISCUSSION

We find that changes in orbital light curve shape can be explained as changes in system parameters, especially those related to the disk and hot/bright spots. The disk is smaller and hotter at long-cycle minimum while it is larger and cooler at long-cycle maximum. The amplitude of the temperature variation is 2840 K, being the minimum reached during the ascending branch. The hot spot has maximum temperature relative to the disk at minimum of the long-cycle while the bright spot does it during the ascending branch. While the hotspot position shows a small variation during the long-cycle with $\lambda_{hs} = 341.5 - 349.2$, the bright spot moves along the disk outer rim during the long-cycle with $\lambda_{bs} = 114.6 - 255.2$. We notice that the hotspot in 7 DPVs is found at λ_{hs} (average) = 327.7 ± 5.6 (std) while the bright spot in the same systems is found in the range $\lambda_{bs} = 107^\circ - 162^\circ$ (Mennickent 2017). This suggests that bright spots tends to occupy broader disk regions than hotspots. In LMC-DPV-97, when the bright spot is opposite to the donor, the secondary eclipse disappears, this happens at long-cycle minimum coinciding with the smaller disk size.

Moving bright spots have been reproduced by 3D simulations of gas dynamics in the cataclysmic variable V 455 And, and interpreted in terms of interactions of a density wave (DW) with shock regions; in this model the DW is in retrograde precession with angular velocity few percent lower than the orbital velocity of the system. As a result, “the times when the density wave interacts with the shocks will be increasing delayed in orbital phase with each successive rotation” (Kononov et al. 2015). Future studies could indicate if this model can be successful for explaining the moving bright spots found in LMC-DPV-97.

We notice that the increase in hotspot angle λ_{hs} is in principle consistent with the increase in disc size, if the hotspot is the site where a free-fall stream hits the disk (Flannery 1975). Even if the stream interacts with a gas envelope forming a hotline in the outer disk border as suggested by Bisikalo et al. (1997), the spread of this region along with the low mass ratio might help to keep small the variability of the λ_{hs} parameter.

5 CONCLUSIONS

We find changes in the orbital light curve of DPV097 linked to the phase of the long-cycle. A preliminary analysis of the light curve indicates that changes in disk size/temperature and spot temperature/position can explain the different observed light curves during the long-cycle. Especially interesting is the result that at minimum of the long-cycle the disk is smaller and hotter and the spots are also hotter, while at maximum the disk is larger and cooler. A more detailed study of this object is in preparation.

Table 2. Results of the analysis of the orbital light curves obtained by solving the inverse problem for the Roche model with an accretion disk around the more-massive (hotter) component.

Quantity	asc	max	des	min
n	370	200	380	387
$\Sigma(O - C)^2$	0.3310	0.0772	0.2439	0.2754
σ_{rms}	0.0299	0.0197	0.0254	0.0267
$i[^\circ]$	74.3	75.1	74.4	74.4
F_d	0.93	0.94	0.68	0.46
T_d [K]	4030	5580	5210	6870
$d_c[a_{orb}]$	0.044	0.034	0.082	0.031
$d_c[a_{orb}]$	0.100	0.110	0.102	0.084
a_T	4.3	6.5	5.9	5.1
F_h	0.242	0.242	0.242	0.242
T_h [K]	14000	14000	14000	1400
T_c [K]	4930	4980	4910	4950
$A_{hs} = T_{hs}/T_d$	1.63	1.70	1.14	1.71
$\theta_{hs}[^\circ]$	19.4	19.1	14.8	23.0
$\lambda_{hs}[^\circ]$	348.6	349.2	340.5	341.6
$\theta_{rad}[^\circ]$	-1.0	-3.6	8.3	2.4
$A_{bs1} = T_{bs}/T_d$	1.78	1.17	1.16	1.76
$\theta_{bs}[^\circ]$	23.3	54.4	26.2	49.0
$\lambda_{bs}[^\circ]$	137.2	114.6	255.2	169.6
Ω_h	8.682	8.699	8.681	8.681
Ω_c	2.233	2.233	2.233	2.233
$\mathcal{M}_h [M_\odot]$	5.51	5.51	5.51	5.51
$\mathcal{M}_c [M_\odot]$	1.10	1.10	1.10	1.10
$\mathcal{R}_h [R_\odot]$	3.65	3.64	3.65	3.65
$\mathcal{R}_c [R_\odot]$	7.75	7.75	7.75	7.75
$\log g_h$	4.06	4.06	4.06	4.06
$\log g_c$	2.70	2.70	2.70	2.70
M_{bol}^h	-1.87	-1.86	-1.87	-1.87
M_{bol}^c	1.03	0.99	1.04	1.01
$a_{orb}[R_\odot]$	30.91	30.91	30.91	30.91
$\mathcal{R}_d[R_\odot]$	15.28	15.40	11.20	7.49
$d_c[R_\odot]$	1.36	1.06	2.53	0.95
$d_c[R_\odot]$	3.09	3.41	3.16	2.6

FIXED PARAMETERS: $q = \mathcal{M}_c/\mathcal{M}_h = 0.20$ - mass ratio of the components, $T_h = 14000$ K - temperature of the more-massive (hotter) gainer, $F_c = 1.0$ - filling factor for the critical Roche lobe of the donor, $f_h = 1.0$; $f_c = 1.00$ - non-synchronous rotation coefficients of the gainer and donor respectively, $\beta_h = 0.25$; $\beta_c = 0.08$ - gravity-darkening coefficients of the gainer and donor, $A_h = 1.0$; $A_c = 0.5$ - albedo coefficients of the gainer and donor.

Quantities: n - number of observations, $\Sigma(O - C)^2$ - final sum of squares of residuals between observed (LCO) and synthetic (LCC) light-curves, σ_{rms} - root-mean-square of the residuals, i - orbit inclination (in arc degrees), $F_d = R_d/R_{yc}$ - disk dimension factor (ratio of the disk radius to the critical Roche lobe radius along y-axis), T_d - disk-edge temperature, d_c , d_c - disk thicknesses (at the edge and at the centre of the disk, respectively) in the units of the distance between the components, a_T - disk temperature distribution coefficient, $F_h = R_h/R_{zc}$ - filling factor for the critical Roche lobe of the hotter, more-massive gainer (ratio of the stellar polar radius to the critical Roche lobe radius along z-axis), T_c - temperature of the less-massive (cooler) donor, $A_{hs,bs} = T_{hs,bs}/T_d$ - hot and bright spots' temperature coefficients, $\theta_{hs,bs}$ and $\lambda_{hs,bs}$ - spots' angular dimensions and longitudes (in arc degrees), θ_{rad} - angle between the line perpendicular to the local disk edge surface and the direction of the hot-spot maximum radiation, $\Omega_{h,c}$ - dimensionless surface potentials of the hotter gainer and cooler donor, $\mathcal{M}_{h,c} [M_\odot]$, $\mathcal{R}_{h,c} [R_\odot]$ - stellar masses and mean radii of stars in solar units, $\log g_{h,c}$ - logarithm (base 10) of the system components effective gravity, $M_{bol}^{h,c}$ - absolute stellar bolometric $a_{orb} [R_\odot]$, $\mathcal{R}_d [R_\odot]$, $d_c [R_\odot]$, $d_c [R_\odot]$ - orbital semi-major axis, disk radius and disk thicknesses at its edge and centre, respectively, given in the solar radius units.

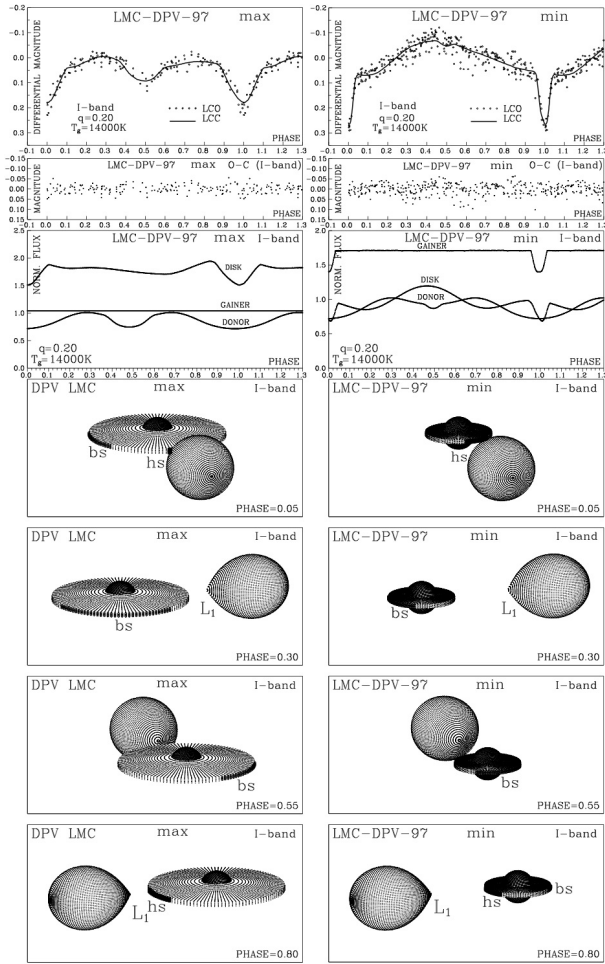


Figure 3. The model compared with observations on the maximum and minimum of the long cycle. Relative flux contributions are in the third panel and representative views of the system at different phases are also given.

6 ACKNOWLEDGMENTS

Thanks to the anonymous referee for providing useful comments that improved the first version of this manuscript. This research has made use of the SIMBAD database, operated at CDS, Strasbourg, France. R.E.M. acknowledges support by VRID-Enlace 216.016.002-1.0 and the BASAL Centro de Astrofísica y Tecnologías Afines (CATA) PFB-06/2007. The OGLE project has received funding from the Polish National Science Centre grant MAESTRO no. 2014/14/A/ST9/00121.

REFERENCES

- Bisikalo D. V., Boyarchuk A. A., Kuznetsov O. V., Chechyotkin V. M., 1997, *ARep*, 41, 786
 Djurašević G., 1992, *Ap&SS*, 197, 17
 Djurašević G., 1992, *Ap&SS*, 196, 267
 Djurašević G., Latković O., Vince I., Cséki A., 2010, *MNRAS*, 409, 329
 Flannery B. P., 1975, *MNRAS*, 170, 325
 Kononov D. A., Bisikalo D. V., Puzin V. B., Zhilkin A. G., Sytov A. Y., 2015, *ARep*, 59, 191
 Marquardt, D. W., 1963, *SIAM*, 11, 431
 Mennickent R. E., 2017, *SerAJ*, 194, 1

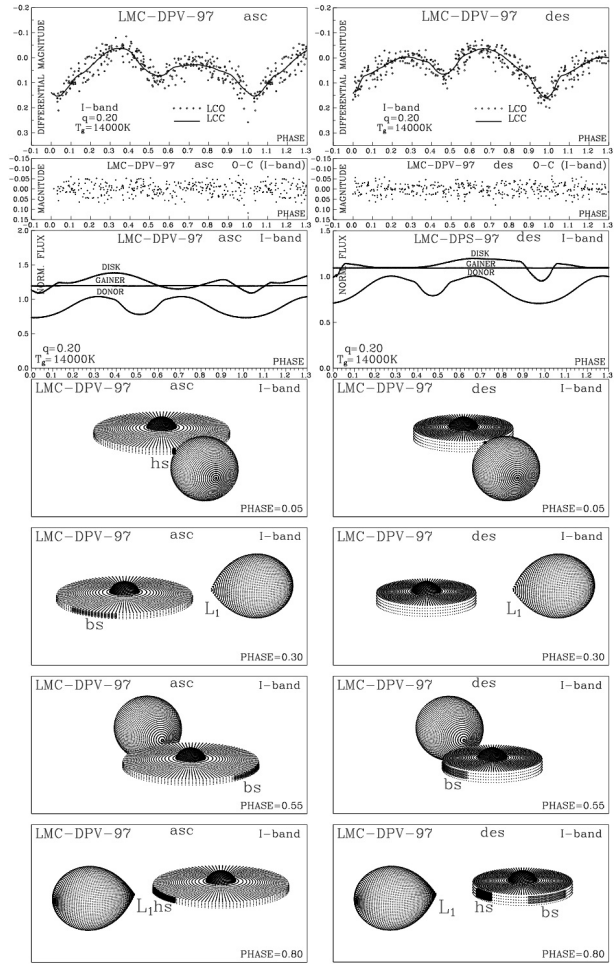


Figure 4. The model compared with observations and residuals on the ascending and descending branches of the long cycle. Relative flux contributions are in the third panel and representative views of the system at different phases are also given.

- Mennickent R. E., Otero S., Kołaczkowski Z., 2016, *MNRAS*, 455, 1728
 Mennickent R. E., Djurašević G., Cabezas M., Cséki A., Rosales J. G., Niemczura E., Araya I., Curé M., 2015, *MNRAS*, 448, 1137
 Mennickent R. E., Kołaczkowski Z., Djurašević G., Niemczura E., Diaz M., Curé M., Araya I., Peters G. J., 2012b, *MNRAS*, 427, 607
 Mennickent R. E., Djurašević G., Kołaczkowski Z., Michalska G., 2012a, *MNRAS*, 421, 862
 Mennickent R. E., Kołaczkowski Z., Michalska G., Pietrzyński G., Gallardo R., Cidale L., Granada A., Gieren W., 2008, *MNRAS*, 389, 1605
 Pawlak M., et al., 2013, *AcA*, 63, 323
 Poleski R., Soszyński I., Udalski A., Szymański M. K., Kubiak M., Pietrzyński G., Wyrzykowski Ł., Ulaczyk K., 2010, *AcA*, 60, 179
 Schleicher D. R. G., Mennickent R. E., 2017, *A&A*, 602, A109
 Udalski A., Szymański M. K. & Szymański G., 2015, *AcA*, 65, 1
 Zola S., 1991, *AcA*, 41, 213